OLGA, A GUST ALLEVIATION SYSTEM FOR IMPROVEMENT OF PASSENGER COMFORT OF GENERAL AVIATION AIRCRAFT

B. Krag, D. Rohlf
Deutsche Forschungs- und Versuchsanstalt für Luft- und Raumfahrt, Institut für Flugmechanik, Braunschweig

H. Wünnenberg
Dornier GmbH, Friedrichshafen

Abstract

The Installation for Dynamic Simulations in Wind Tunnels of the DFVLR was used, to test a gust alleviation system under nearly realistic environmental conditions. A remotely controlled, dynamically scaled wind tunnel model of the ZKP-experimental aircraft was used as a test bed. Like a real aeroplane this model was equipped with all necessary sensors for an on-board measurement of the motion parameters.

Using this wind tunnel model, an open loop gust alleviation system was investigated. The aim of these experiments was a total compensation of the gust induced lift and pitching moment by an optimal adjustment of the parameters. Also several experiments were performed, to verify the motion parameters of the model and the accuracy of the sensors by application of parameter identification methods. Finally, the influence of measuring accuracy, gust sensor position, control surface rate limitation and the dynamic characteristic of the sensors on the performance of the gust alleviation system and the handling qualities of the model was investigated by systematic parameter variations.

For these investigations a scaled two dimensional stochastic gust field was generated in the test section of the wind tunnel. The results obtained from these wind tunnel experiments are subject of this paper.

List of Symbols

T	Time delay
V_o	Stationary velocity of the aeroplane
x	Distance
α	Angle of attack
$\bar{\alpha}$	Angle of attack obtained from measurements
η	Elevator deflection
δ	Symmetric aileron deflection
ε	Downwash factor

Indices

e	Effective
E	Elevator
G	Gust
k	Kinematic
V	Vane
VE	Vane-Elevator
VW	Vane-Wing
W	Wing
WE	Wing-Elevator
δ	Symmetric aileron deflection

1. Introduction

An experiment may have two different meanings: to gain knowledge of the physical process under observation on one side or to verify a result, which has been obtained on a pure theoretical way on the other side.

The expense for the experiment depends on the problem to be investigated. The number of parameters should be kept as low as possible, so that the result only depends on a few variables. Accordingly the Installation for Dynamic Simulation in Wind Tunnels of the DFVLR-Braunschweig was used, to develope and test a gust alleviation system. This gust alleviation system was designed for a small civil transport aeroplane, to improve the ride comfort of the passengers. The wind tunnel experiments helped to find a correct mathematical model of the aeroplane flying in a two-dimensional gust field. The wind tunnel experiments also showed the conditions, which are necessary for a good performance of the gust alleviation system. The experiments gave a profound insight into the interaction of the downwash with the gusts, which arrive at different moments at the position of the wing and the elevator. These results at least will give valuable data for the construction of the gust alleviation system for the full scale aeroplane.

2. The Installation for Dynamic Simulation in Wind Tunnels

The Installation for Dynamic Simulation in Wind Tunnels was designed for the estimation of the aircraft stability derivatives and for the testing of active control systems[1,2,3]. Within certain limitations portions of the flight envelope can be simulated in the wind tunnel for a variety of aeroplanes. These constraints are given by the observance of the laws of similarity[4], and by the limited freedom of movement in the wind tunnel. The Installation for Dynamic Simulation consists of three main parts (Figure 1): A large suspension frame for the model, a model control- and data processing station and a gust generator.

The model is allowed to move free on a vertical bar. This type of suspension allows the vertical motion, pitching -, yawing - and rolling motion.

The model is a 1 : 8 replica of the Do 28 TNT aeroplane and is scaled to the cruising condition (Figure 2). The model is built from carbon-fiber material and is equipped with electric fast moving servo actuators for all control surfaces. Additionally a variety of sensors are installed to measure the motion parameters, accelerations and the angle of attack (Figure 3). The gust generator consists of two moveable flaps, which are installed into the nozzle of the wind tunnel. These flaps are driven by an electrohydraulic servoactuator. The gust field is nearly two dimensional, and there is a slight increase of the gust amplitude downstream of the nozzle. Within a certain bandwidth of frequencies, the gust amplitude remains constant. Beyond this band of frequencies, instationary aerodynamic effects produce a complicated dependence of the gust amplitude from the frequency (Figure 4).

The Installation for Dynamic Simulation can be used to simulate the longitudinal motion of an aeroplane. The phugoid motion is suppressed by the blockage of the x-degree of freedom. Correct Froude-number simulation can be achieved by a weight-alleviation system, which applies a constant vertical force to the model. Despite of all restrictions, the Installation for Dynamic Simulation, together with a computer simulation, turned out to be a good tool to solve the problems in the connexion with the gust alleviation.

3. Dynamic Response Investigations

The wind tunnel investigations began with a series of extensive experiments for the identification of the model motion parameters. These experiments served to complete and correct the mathematical description of the model response and to detect hitherto unknown effects which had to be included into the mathematical model. For the purpose of parameter identification, the model was excited by impulsive deflections of the control surfaces and the gust generator flaps. A variety of frequency response measurements were performed, either by harmonic oscillating control surfaces or by flying in a harmonic oscillating gust field. For some experiments, the model was fixed at the center of gravity, so that only the pitching motion was allowed.

The mathematical model, which describes the motion of the model in the wind tunnel had to include a lot of terms, which are correlated directly to the influence of the test facility on the model motion. These disturbing influences include friction at the bar, friction and additional pitching moments caused by the cables, nonlinear propagation of the gust field, interaction of the large tubular suspension-frame with the airflow around the model, etc. Figure 5 shows the response of the model, following an impulsive elevator deflection. There is a good agreement between the measured response in the wind tunnel and the computed response of the mathematical model. Figure 6 shows frequency response measurements of the vertical acceleration. The model was excited by harmonic elevator and symmetric aileron deflections. Both responses show a good agreement between measurement and computation not only with the amplitudes but also with the phases. This agreement shows, that the parameters, which describe the motion of the model, have been estimated with considerable accuracy. Of more concern was the mathematical modelling of the propagation of the gust field. Figure 7 shows the gust angle of attack following an impulsive deflection of the gust generator flaps. The response indicates a complicated aerodynamic process. The frequency response measurements of the gust angle of attack at three different positions downstream of the nozzle show two fundamental frequencies. The first frequency at 3.7 Hz is correlated to the wind tunnel resonance and a second characteristic frequency appears at about 9 Hz. The source for the last frequency still is not fully detected. A simple mathematical model was developed, which takes into account of the two characteristic frequencies. The model bases on the assumption, that there exists a bound vortex in the quarter-chord-line of the gust-flap and that an indicial vortex moves downstream from the trailing edge of the gust flap. Comparing the measured and computed gust angle of attack responses, the deficiencies of this simple model are evident. Figure 8 shows the response of the model following an impulsive deflection of the gust generator flaps. Despite inaccurate modelling of the gust-field, there is a good agreement between measured and computed response. Figure 9 shows a frequency response of the vertical acceleration in a harmonically oscillating gust field. Here we see, that within a frequency band of 0.8 Hz to 5 Hz the computation of the response is accurate. Below 0.8 Hz the model response decreases compared with the computation. In this low frequency regime not accurately realized friction effects may be the cause. Above of 5 Hz the propagation of the gust field is responsible for a distinct minimum at 7 Hz. Here the mathematical model failes completely.

The gust generator is a servo system, so that also stochastic input signals could be applied. Using an analog shaping-filter, gust fields with a v. Karman- or Dryden-characteristic could be generated. Figure 10 shows the power-spectra of the Dryden-shaping-filter-output, the measured and the computed spectra for the gust angle of attack. The measured spectrum shows a distinct resonance peak at 3.7 Hz. Above of 5 Hz, the spectral density of the

gust amplitude remains constant. This is caused by the large natural turbulence of the wind tunnel. Figure 11 shows the power spectrum of the vertical acceleration. It shows the same features like the frequency response of the vertical acceleration. The distinct minimum at 7 Hz has disappeared because the excitation by the natural turbulence becomes dominating.

Despite of some deficiencies in the modelling of the gust field, a frequency band exists, where a good agreement between measurement and computation exists. Within this frequency band, from 0.8 Hz to 5 Hz, the results from measurement and computation are valid in the same manner. The results from investigations with a gust alleviation system, which are presented here, therefore were obtained either from measurements or from computations.

4. The Open Loop Gust Alleviation System (OLGA)

For the Do 28 TNT transport aeroplane, the DFVLR chose the open loop gust alleviation system. This gust alleviation system shall improve the ride comfort of the passengers during the cruising condition. This system has the advantage, that the time which the gust needs to pass the distance from the angle of attack vane to the wing, can be used to compensate the actuator lag. In this way most benefits out of the lift creating capability of the symmetric deflecting ailerons can be obtained. For better understanding of the operation of the gust alleviation system, the equations of motion are given. The equations of motion are given in wind tunnel fixed axes. The formulation follows the lines given in[5].

$$\ddot{x} = X_{\alpha_W}\alpha_W + X_{\alpha_E}\alpha_E + X_\eta \eta + X_{\delta_W}\delta$$

$$\ddot{z} = Z_{\alpha_W}\alpha_W + Z_{\alpha_E}\alpha_E + Z_\eta \eta + Z_{\delta_W}\delta \qquad (4.1)$$

$$\ddot{\theta} = M_{\alpha_W}\alpha_W + M_{\alpha_E}\alpha_E + M_\eta \eta + M_{\delta_W}\delta$$

For the matter of simplicity all wind tunnel specific effects are excluded from the equations. The angles of attack at the vane, wing and the elevator are:

$$\alpha_V = \frac{1}{V_o}\dot{z} + \theta - \frac{x_V}{V_o}\dot{\theta} + \alpha_G$$

$$\alpha_W = \frac{1}{V_o}\dot{z} + \theta + \frac{x_W}{V_o}\dot{\theta} + \alpha_G(t - T_{VW}) \qquad (4.2)$$

$$\alpha_E = \frac{1}{V_o}\dot{z} + \theta + \frac{x_E}{V_o}\dot{\theta} - \varepsilon_W \alpha_W(t - T_{WE}) - \varepsilon_\delta \delta(t - T_{WE}) + \alpha_G(t - T_{VE})$$

The time delays T are given by the velocity of the aeroplane and the distances of the vane, wing and elevator. Because the gust alleviation system is operating only in the cruising condition, the velocity remains constant and the time delays do not change. During the wind tunnel experiments with the Do 28 TNT model it became apparent, that the adjustment of the gust alleviation system could be facilitated, if the problem is divided into a stationary part and an instationary part. According to ref.[6], we define the dynamic angle of attack as follows:

$$\alpha^*(t) = \alpha(t - T_{WE}) - \alpha(t) \qquad (4.3)$$

The equations for the angles of attack contain the kinematic angle of attack at the center of gravity

$$\alpha_k = \frac{1}{V_o}\dot{z} + \theta \qquad (4.4)$$

The gust angle of attack is measured relative to the position of the angle of attack vane. Introducing Equ. (4.3) and (4.4) into Equ. (4.2) we have:

$$\alpha_V = \alpha_k - \frac{x_V}{V_o}\dot{\theta} + \alpha_G$$

$$\alpha_W = \alpha_k + \frac{x_W}{V_o}\dot{\theta} + \alpha_G(t - T_{VW}) \qquad (4.5)$$

$$\alpha_E = (1 - \varepsilon_W)\alpha_k - \varepsilon_W \alpha_k^* + \frac{1}{V_o}(x_E - \varepsilon_W x_W)\dot{\theta} - \varepsilon_W \frac{x_W}{V_o}\dot{\theta}^* - \varepsilon_\delta(\delta + \delta^*) + (1 - \varepsilon_W)\alpha_G(t - T_{VW}) + (1 - \varepsilon_W)\alpha_G^*$$

Using Equ. (4.5) the coefficients in Equ. (4.1) can be summed up to form the derivatives for the total aeroplane. This is advantageous, because total derivatives are known more precisely from wind tunnel measurements than the single coefficients of the separated wing and elevator. In this way we find for the total derivatives of the Z-equation for example:

$$Z_\alpha = Z_{\alpha_W} + (1 - \varepsilon_W)Z_{\alpha_E}$$

$$Z_q = Z_{\alpha_W}\frac{x_W}{V_o} + Z_{\alpha_E}\left(\frac{x_E}{V_o} - \varepsilon_W \frac{x_W}{V_o}\right) \qquad (4.6)$$

$$Z_\delta = Z_{\delta_W} - \varepsilon_\delta Z_{\alpha_E}$$

In a quite similar way, the total derivatives for the other equations can be found. Following, the equations of motion are divided into a stationary part and an instationary part.

$$\ddot{x} = X_\alpha \alpha_k + X_\delta \delta + X_\eta \eta + X_\alpha \alpha_G(t - T_{VW}) + X_q \dot{\theta} - X_{\alpha_E} \varepsilon_W \alpha_k^* - X_{\alpha_E} \varepsilon_W \frac{x_W}{V_o} \dot{\theta}^* - X_{\alpha_E} \varepsilon_\delta \delta^* + X_{\alpha_E} (1 - \varepsilon_W) \alpha_G^*$$

$$\ddot{z} = Z_\alpha \alpha_k + Z_\delta \delta + Z_\eta \eta + Z_\alpha \alpha_G(t - T_{VW}) + Z_q \dot{\theta} - Z_{\alpha_E} \varepsilon_W \alpha_k^* - Z_{\alpha_E} \varepsilon_W \frac{x_W}{V_o} \dot{\theta}^* - Z_{\alpha_E} \varepsilon_\delta \delta^* + Z_{\alpha_E} (1 - \varepsilon_W) \alpha_G^* \quad (4.7)$$

$$\ddot{\theta} = M_\alpha \alpha_k + M_\delta \delta + M_\eta \eta + M_\alpha \alpha_G(t - T_{VW}) + M_q \dot{\theta} - M_{\alpha_E} \varepsilon_W \alpha_k^* - M_{\alpha_E} \varepsilon_W \frac{x_W}{V_o} \dot{\theta}^* - M_{\alpha_E} \varepsilon_\delta \delta^* + M_{\alpha_E} (1 - \varepsilon_W) \alpha_G^*$$

According to these equations, the gust alleviation system was developed. Figure 12 shows a block-diagram of the open loop gust alleviation system. The disturbance signal is computed from the angle of attack and the aircraft motion parameters. The desired dynamic portion of the signal is obtained by filtering with a time delay filter and following subtraction from the gust signal. The objective of the gust alleviation system is the complete compensation of the gust-induced lift and pitching moment. Accordingly the gust compensation follows the following control law[7]:

1. Compensation of the stationary portions:
   - symmetric aileron deflection δ for the compensation of the additional lift, which is given by the gust induced lift of the total aeroplane and by an elevator deflection η_1.
   - simultaneous elevator deflection η_1 for the compensation of the pitching moment due to the gust and due to the symmetric aileron deflection δ.
2. Compensation of the dynamic portions:
   - elevator deflection η_2 for the compensation of the additional lift at the elevator due to the dynamic portions of the gust and aileron deflection.
3. Superposition of the portions:

$$\eta = \eta_1 + \eta_2 \quad (4.8)$$

The gain-factors, which are necessary for the compensation, result from the following conditions:

Stationary portions:

$$Z_\alpha \alpha_G (t - T_{VW}) + Z_\delta \delta + Z_\eta \eta_1 = 0$$
$$M_\alpha \alpha_G (t - T_{VW}) + M_\delta \delta + M_\eta \eta_1 = 0 \quad (4.9)$$

Dynamic portions:

$$Z_{\alpha_E} (1 - \varepsilon_W) \alpha_G^* - Z_{\alpha_E} \varepsilon_\delta \delta^* + Z_\eta \eta_2 = 0$$
$$M_{\alpha_E} (1 - \varepsilon_W) \alpha_G^* - M_{\alpha_E} \varepsilon_\delta \delta^* + M_\eta \eta_2 = 0 \quad (4.10)$$

Both equations for the consideration of the dynamic portions are equivalent. During the wind tunnel experiments we found, that the gust alleviation system was very sensitive with regard to deviations from the correct pitching moment value. Therefore the pitching moment coefficients should be estimated very carefully and the last equation of Equ. (4.10) should be used to calculate the elevator deflection η_2. The following control surface deflections for the gust compensation result from Equs. (4.9) and (4.10):

$$\delta = - \frac{M_\eta Z_\alpha - M_\alpha Z_\eta}{M_\eta Z_\delta - M_\delta Z_\eta} \alpha_G(t - T_{VW}) \quad (4.11)$$

$$\eta = \frac{M_\delta Z_\alpha - M_\alpha Z_\delta}{M_\eta Z_\delta - M_\delta Z_\eta} \alpha_G(t - T_{VW}) \quad (4.12)$$
$$- \frac{M_{\alpha_E}}{M_\eta} \left[(1 - \varepsilon_W) - \varepsilon_\delta \frac{M_\eta Z_\alpha - M_\alpha Z_\eta}{M_\eta Z_\delta - M_\delta Z_\eta} \right] \alpha_G^*$$

Inaccurate knowledge of the derivatives nessitated a number of special experiments to adjust the gain factors for the stationary and the dynamic gust compensation. A similar technique also has to be used for the adjustment of the gust alleviation system for the full-scale aeroplane. The optimal adjustment was found by observing the motion of the model and by observing the vertical acceleration. The vertical acceleration was filtered by a special filter, which is weighting those frequencies, which are unpleasant for the passengers (Figure 13). There are especially the frequencies below 0.5 Hz, which are responsible for the motion sickness.

The performance of the gust alleviation system is affected by a number of deficiencies. These are given by the

- maximum deflection of the aileron, which is permitted for the gust compensation
- maximum control surface deflection rates
- inertial properties of the angle of attack vane
- accuracy of the computation of the gust signal

- backlash and other nonlinearities of the actuators.

Because all dynamic systems in the control loop have a low-pass characteristic, the performance of the gust alleviation system decreases with increasing gust frequency. The exact gust-compensation presupposes a correct deflection of the control surfaces without any phase-lag relative to the gust frequency. This can be achieved, by taking advantage of the time-delay T_{VW}, which allows for the compensation of the phase lag of the actuators, vane and filters. Actually, this is valid only for one distinct frequency as indicated in Figure 14. The amplitude - and phase characteristic of a low pass system are different from the pure time-delay. If there is more phase-reserve available, than is already used for the compensation of phase-lags within the control-loop, this residual phase-lag has to be compensated by a filter. During the wind tunnel experiments, a digital time-delay filter turned out to be a practical solution. The time-delay filter can be easily tuned, so that the maximum gust alleviation occurs at the desired frequency. Figure 15 shows the frequency response of the vertical acceleration with the gust alleviation system engaged. The minimum of the acceleration appears at a frequency of 1.2 Hz. Because there is a time scale factor of 2.4, the minimum for the full scale aeroplane would appear at 0.5 Hz. Figure 16 shows the time histories of the wind tunnel model and the mathematical model. $\bar{\alpha}_G$ is the gust signal, computed from the vane-signal. The accelerations b_y and $\ddot{z}$ are well suppressed by the gust alleviation system. b_y is the acceleration at the cockpit station. The good alleviation at both stations, cockpit and center of gravity, indicates also a good suppression of the pitching acceleration. Compared with the computations, the measurements show much more disturbance. This is caused by the uncorrelated wind tunnel turbulence, to which the gust alleviation system does not respond. Comparing the control surface-deflection, we see, that during the experiments we used larger aileron deflections. The elevator deflection does not follow the gust signal in the way it does during the computation. This indicates, that the optimal setting of the gains was not achieved. Figure 17 shows the power spectra of the vertical acceleration. The wind tunnel resonance peak at 3.7 Hz is evident. Below 0.2 Hz there is no excitation of the model, because the input signal of the noise generator does not contain these low frequencies. Despite the fact, that the optimal adjustment of the gust alleviation system was not found completely, Figure 18 shows, that there is no deterioration of the handling qualities. There are no differences between the responses of the aeroplane with and without the gust alleviation system. This indicates no feedback of the aircraft motion parameters.

5. Influence of Parameter Variations on the Performance of the Gust Alleviation System

The parameters, which affect the performance of the gust alleviation system, already have been mentioned in the preceding chapter. They were the subject for investigations in the wind tunnel and on the computer.

5.1 Vertical Speed

The accurate estimation of the gust signal is necessary in an open loop gust alleviation system. Otherwise portions of the motion parameters would be fed back and would deteriorate the handling qualities. Figure 19 shows two possible ways to obtain the desired gust signal[8]. Generally, small transport aeroplanes are not equipped with inertial platforms. Therefore the vertical speed has to be estimated by a simple strap-down device or by an estimation filter. Both ways give a vertical speed signal, which is accurate only within a certain bandwidth. The effect of $\dot{z}$-limitation was investigated at first. The $\dot{z}$-signal was suppressed by low-pass filters with different corner frequencies. The gust signal results from the first equation of Equ. (4.2)

$$\alpha_G = \alpha_e - \frac{1}{V_o}\dot{z} - \theta + \frac{x_V}{V_o}\dot{\theta} \qquad (5.1)$$

α_e is the effective angle of attack at the position of the vane. On board of the aeroplane sensors and filters are used to estimate the gust signal and only a limited accuracy can be achieved:

$$\bar{\alpha}_G = \alpha_V - \frac{1}{V_o}\bar{\dot{z}} - \bar{\theta} + \frac{x_V}{V_o}\bar{\dot{\theta}} \qquad (5.2)$$

Equation (5.1) and Equ. (5.2) only agree within a distinct domain of frequencies. Each filtering of a signal component will narrow down this domain. As mentioned previously, the conditions for total compensation can be met for technical reasons only at one distinct frequency. So it will be appropriate to obtain accurate gust-signal computation, according to Equ. (5.2), especially for this frequency. An additional filter, introduced before the summation point for suppressing signal noise, will change the phase and amplitude of one of the gust-signals components. A restoration of the correct amplitude by increasing the gain will result in a faulty summation for the lower frequencies. The experience in the wind tunnel has shown, that each manipulation of the signals before the summation point in order to obtain a good adjustment for one specific frequency, always results in a degradation of the gust alleviation. If filtering is necessary, it has to be done after the summation point. This can be demonstrated effectively by observing Figure 20.

The ż-signal was superimposed with white noise. This deteriorates the gust alleviation in the whole frequency domain. Filtering of ż gives no improvement, because Equ. (5.2) is hurt. On the contrary, the strong phase shift of the low-frequency filter excites the vertical acceleration. Filtering of the complete gust signal after the summation point and the following adjustment of the gain-factors of the gust alleviation system enables a sufficient gust alleviation in the lower frequency domain. Fig. 21 shows the results obtained from the wind tunnel experiments. Filtering of the ż-signal produces a distinct oscillatory motion of the model.

5.2 Pitch Attitude

The open loop gust alleviation system is designed for a stationary flight condition. So the gust compensation (suppression of the disturbance) will restore the stationary flight condition. The stationary flight condition is characterized by the stationary angle of attack. In the wind tunnel this is identical with the stationary pitch attitude Θ. If the pitch attitude cannot estimated accurately, the gust alleviation system is not able to restore the stationary flight condition. The aeroplane will drift slowly up or down. However it is possible to suppress this divergent motion by wash-out-filtering of the gust signal. There is still another reason for the introduction of a wash-out-filter. This filter also shall suppress the zero-offsets of the sensors. Engaging the gust alleviation system, zero-offsets could produce an undesired control-surface deflection.

Normally the pitch attitude is measured by attitude-gyros. Attitude gyros are not considered for the full scale aeroplane. Consequently the pitch attitude has to be obtained by a special estimation filter or by integration of the pitch-rate signal. The latter way is interesting because it is more simple.

An exact integration of the pitch-rate signal is not possible, because small offsets gradually are integrated to large values. Therefore a stabilized approximate integration is preferred, as indicated in Fig. 19. The corner-frequency of the integrator has to be sufficiently below the domain of interesting frequencies. On the other side it has to be large enough, in order to obtain a quick response of the system. The effects of the integrator time-constants and high-pass filter corner-frequencies have been investigated. During the wind tunnel experiments, the absence of a high-pass (wash-out) filter always resulted in a slow divergent motion of the model. Figure 22 shows the effect of high-pass filtering for a given integrator time-constant. The high-pass filter produces a phase lead of the gust signal. This is equivalent to a magnification of the residual time-delay. Accordingly the condition for optimal gust compensation is shifted to other frequencies. If the integrator time-constant is badly chosen, this will give a poor Θ-signal for some frequency. An adjustment of the gust-signal, according to the lower part of Fig. 22, will result in a worse gust alleviation system. Fig. 23 shows the drifting of the wind tunnel model, when the integrator and the high-pass filter are not optimally tuned. Following an impulsive elevator deflection, a pitch angle slowly builds up. The integrated pitch-rate signal however remains constant. The gust-signal is poor and there is a feedback of the pitch-attitude via the ailerons. For example complete stable conditions could be achieved with a corner-frequency of a factor ten smaller than the interesting frequency. Conditions also improved with higher-order high-pass filters. The effect of such an arrangement is shown in Fig. 24. The relative large phase shift of the high-pass filter (3rd order Butterworth-filter) shifted the minimum to a higher frequency, more than a second order low pass filter would have done. Recentering of the minimum to the desired frequency could be achieved by adjusting the residual time-delay and the gain-factors. The system was stable, but the gust alleviation was worse as compared with the adjustments in Fig. 22. Besides large control surface deflections were produced. That indicates, that the compensation of the large phase shifts, produced by higher order filters, always leads to a poor performance of the gust alleviation system. Fig. 22 showed some good combinations of integrator time constants and high-pass filter corner frequency. As a rough recommendation the corner frequencies of a second order high pass filter and a first order integrator should be smaller by a factor ten than the lowest interesting frequency of the dynamic system.

5.3 Control Surface Deflection Rate Limitation

Hydraulically or electrically operated control surface actuators only can produce a limited deflection rate. This has a profound effect on the performance of the gust alleviation system. Reasons of expense do not permit the installation of high performance electro-hydraulic actuators into the small transport aeroplane. Therefore the rate limitation severely influences the choice of the actuator. Simulations with different deflection rate limitations have shown, that for deflection rates $> 60\ ^{o}/s$ deteriorations only occur in the higher frequency domain. For deflection rates smaller than $60\ ^{o}/s$ also the distinct minimum begins to disappear. This indicates, that under nonlinear conditions the simple phase relationship between time-delay and actuator phase-lag is no longer valid. Under these nonlinear conditions an adjustment of the gust alleviation system for one specific frequency is difficult. Fig. 25 shows the effect of three different aileron deflection-rate-limitations.

The position of the minima is slightly different, because the gain-factors have been changed. The frequency response for $\dot{\delta}_{max}$ = 36 °/s clearly shows a deterioration of the gust alleviation throughout the whole frequency-domain. The simulations have shown, that the deflection rates should not be reduced below values of 60 - 70 °/s. A rough estimation of the necessary maximum deflection rate is given by

$$\dot{\delta}_{max} \approx \omega \, \delta_{max} \qquad (5.3)$$

ω is the upper boundary of the frequency domain, where good gust alleviation is demanded. δ_{max} is the maximum permissible control surface deflection for the gust alleviation.

5.4 Limitation of the Gust Signal and Back-Lash

The block diagram of the gust alleviation system (Fig. 12) shows a limiter for the α_G-signal. In the case the gust signal commands too large aileron deflections, these would reach the deflection limits (point of saturation). On the other hand, because the elevator deflections are smaller by a factor ten, they are far away from their deflection limits, so producing pitching motions. The limiter prevents the model getting out of balance if more than the maximum aileron deflection is commanded. Fig. 26 (left side) shows the effect of the gust signal limitation for the case of a harmonically oscillating gust field of 1 Hz. The limitation affects the quality of the gust alleviation especially in the domain of higher frequencies.

Another source for the deterioration of the gust alleviation is given by the back lash within the aileron driving mechanism. Fig. 25 (right side) shows the effect of aileron back lash for a harmonically oscillating gust field of 1 Hz. For the purpose of investigation, the back lash of the aileron was given a fairly large value. Despite of this large back lash the gust alleviation is acceptable. This indicates, that some back lash can be tolerated by the gust alleviation system. All attempts to improve the gust alleviation by adjusting the gain factors will result in a worse gust alleviation. If there is some back lash, the parameters of the gust alleviation system may not be changed.

6. Conclusions

Using a remotely controlled wind tunnel model and by computer simulations an open loop gust alleviation system (OLGA) for a small civil transport aeroplane was investigated. During the wind tunnel experiments two goals were persued: First, the thoroughly identification of the motion parameters of the model, an investigation of the gust field propagation in the wind tunnel and the estimation of all influences from the wind tunnel installations upon the model motion. Secondly, the gust alleviation system was transferred to the model and adjusted optimally. Afterwards the influence of several parameters on the performance of the gust alleviation system was investigated by a number of specific experiments in the wind tunnel. All wind tunnel experiments were supplemented by computer simulations.

The investigations showed, that an open loop gust alleviation system for a small transport aeroplane could be very efficient, if a number of fundamental relations are considered:

- The estimation of the disturbance, which should be compensated by the gust alleviation system, has to be rather accurate.
- The phase shift between original and measured pitch angle should be less than 5 deg. within the frequency domain of interest.
- Noise filtering of the motion sensor signals should not be accomplished before the computation of the gust signal.
- For the suppression of integration errors, wrong initial conditions and sensor offsets a high-pass filter of low order can be recommended. But the corner frequency of this filter should be lower by a factor of ten than the lowest frequency considered for the gust alleviation.
- The time-delay, which is given by the forward position of the angle of attack vane, can be favourably used for the compensation of actuator and filter lags.An adjustable time-delay filter can be used for the compensation of the eventually remaining time-delay.
- The compensation of filter and actuator lags by using the available time-delay only is accurate in the lower frequency domain. Within the domain of higher frequencies the phase shift of the time delay exceeds the phase shift produced by systems with low pass characteristic. Therefore adjustments of the gust alleviation system should be accomplished only in the lower frequency domain.
- Control surface deflection rate limitation means a frequency dependent degradation of the gust alleviation. For very small deflection rate limitations, an adjustment also for low frequencies becomes difficult and the condition for exact compensation for at least one frequency no longer can be achieved.
- Small back lash as it is common with off-the-shelf equipment does not affect the performance of the gust alleviation system significantly. Readjustment of the gain factors in order to compensate for the back lash effects always will not improve the results.

7. References

1. Subke, H. and Krag, B.: Dynamic Simulation in Wind Tunnels, Part II. AGARD CP-187, 1975.

2. Krag, B.: Gust-Vehicle Parameter Identification by Dynamic Simulation in Wind Tunnels. AGARD CP-235, 1978.

3. Hamel, P.G. and Krag, B.: Dynamic Windtunnel Simulation of Active Control Systems. AGARD CP-260, 1978.

4. Subke, H.: Test Installations to Investigate the Dynamic Behaviour of Aircraft with Scaled Models in Wind Tunnels. Trans. Inst. MC 1, No. 3, July - Sept. 1979.

5. Krag, B.: Active Control Technology for Gust Alleviation. v. Karman Institute for Fluid Dynamics, Lecture Series on Active Control Technology, December 4 - 8, 1978.

6. Krag, B. and Rohlf, D.: Equations of Motion of the Do 28 TNT-Model. DFVLR IB 154-79/16, 1979.

7. Rohlf, D.: Bewegungsgleichungen und modifiziertes Open-Loop-Böenabminderungssystem für das Do 28 TNT-Windkanalmodell. DFVLR IB 154-79/17, 1979.

8. Brockhaus, R., Wüst, P., Barth, R. and Lonn, E.: Entwurf und Erprobung von Schätzverfahren zur Ermittlung von Wind- und Böenstörungen zur Störgrößenkompensation. BGT TB OOOD 1264/1977.

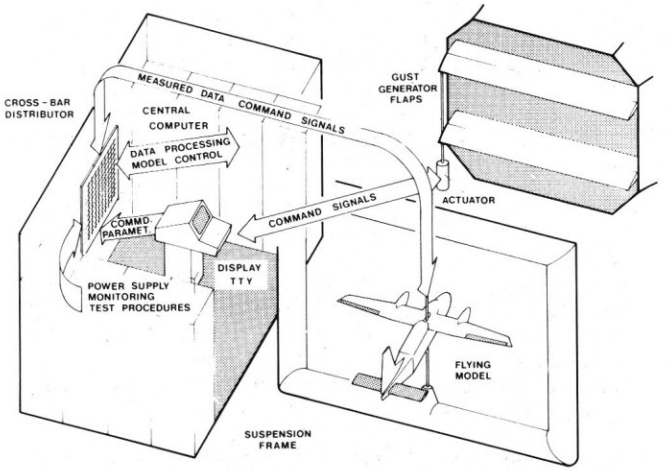

Figure 1. General view of the installation for dynamic simulation in wind tunnels.

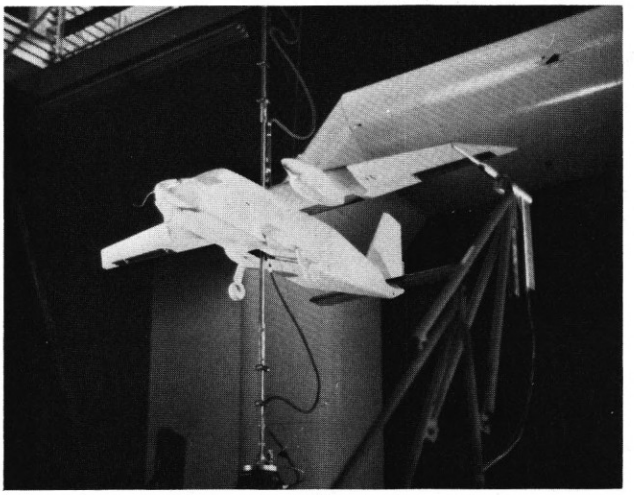

Figure 2. Remotely controlled wind tunnel model of the Do 28 TNT.

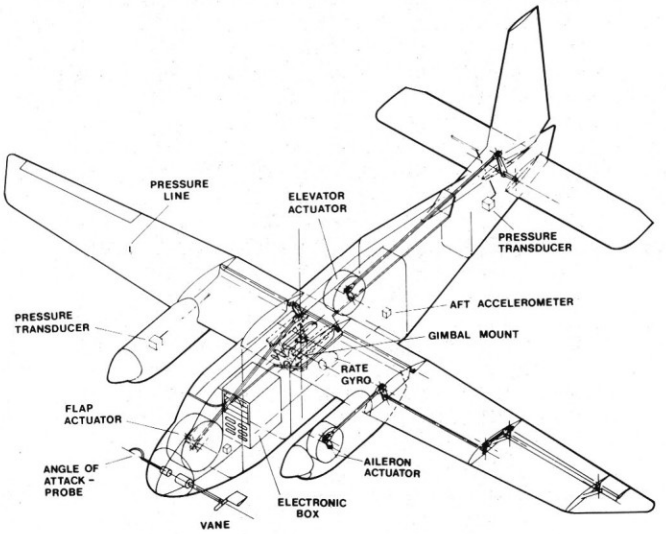

Figure 3. Equipment of the Do 28 TNT wind tunnel model.

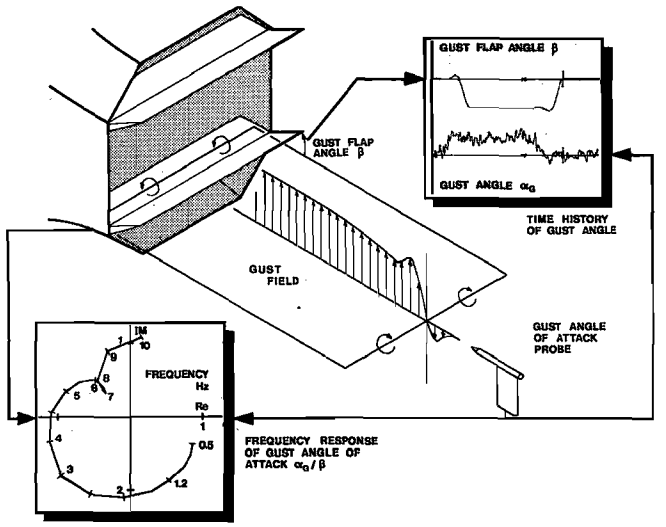

Figure 4. Gust generator and aerodynamic properties of the artificial gust field.

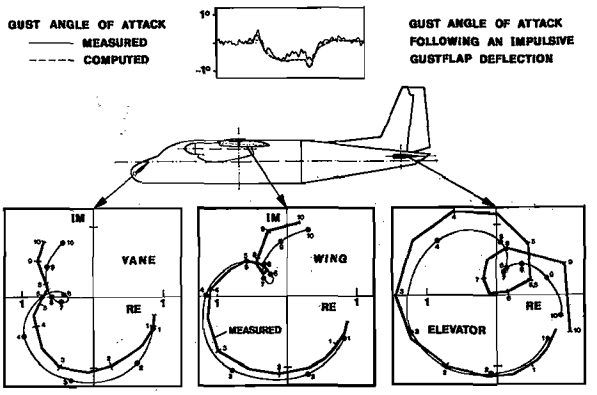

Figure 7. Measured and computed frequency response of the gust angle of attack at three positions.

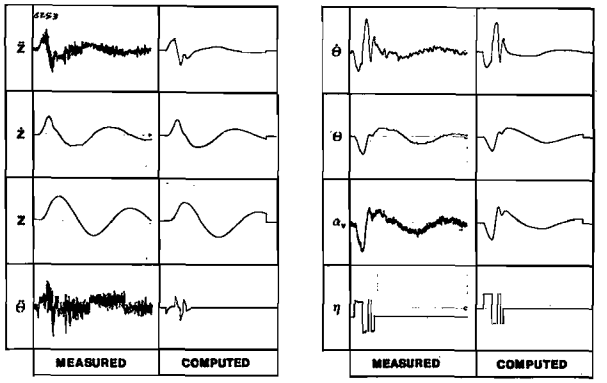

Figure 5. Comparison of measured and computed response to an impulsive elevator deflection.

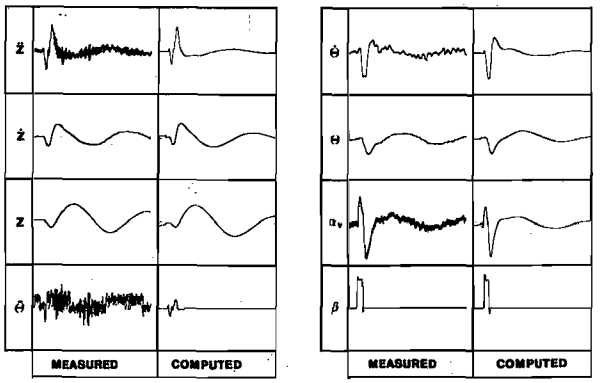

Figure 8. Comparison of measured and computed response to an impulsive gust flap deflection.

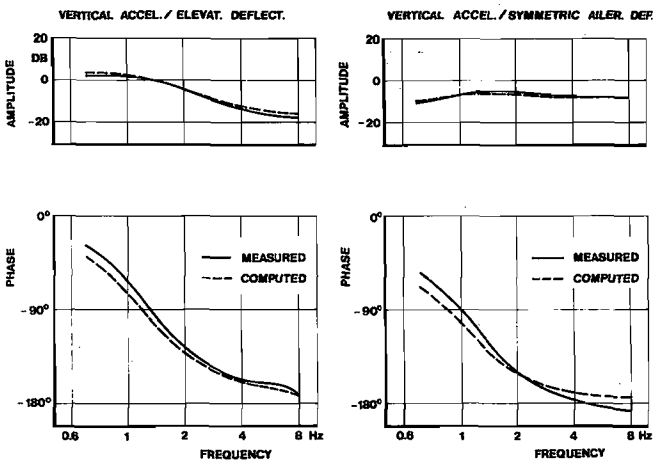

Figure 6. Comparison of measured and computed frequency responses.

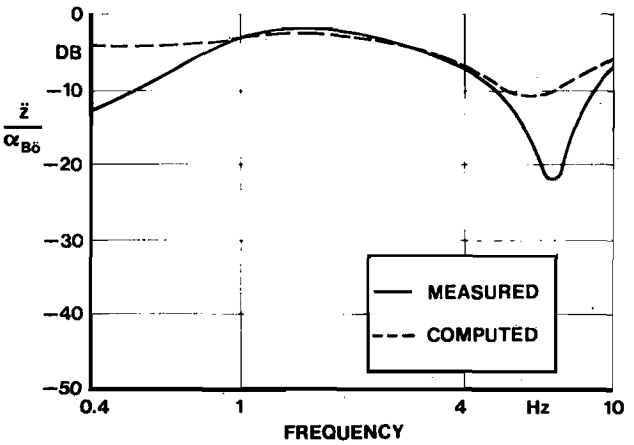

Figure 9. Frequency response of the vertical acceleration to a harmonically oscillating gust field.

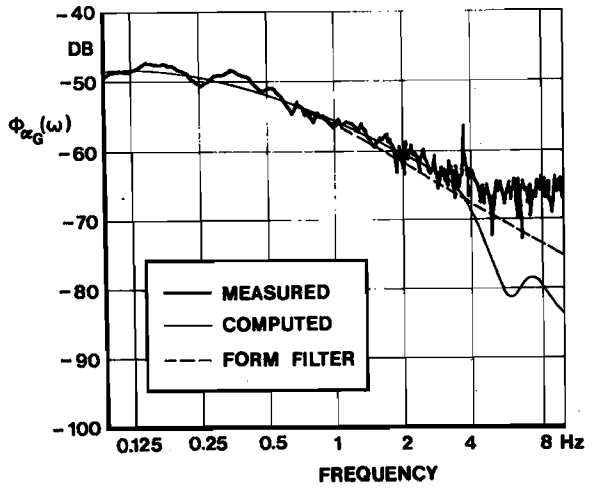

Figure 10. Measured and computed power spectrum of the gust angle of attack in a scaled stochastic gust field with Dryden-characteristic.

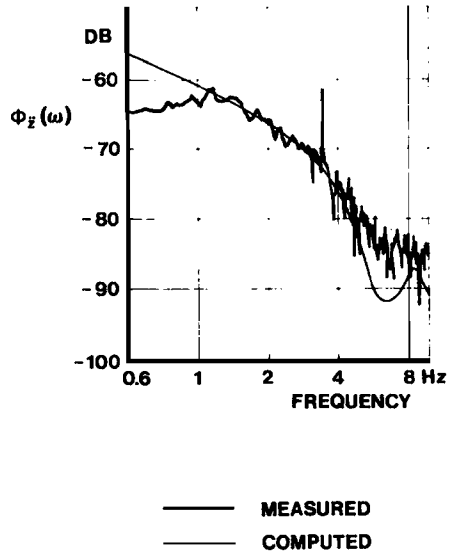

Figure 11. Measured and computed power spectrum of the vertical acceleration during flight through a scaled stochastic gust field.

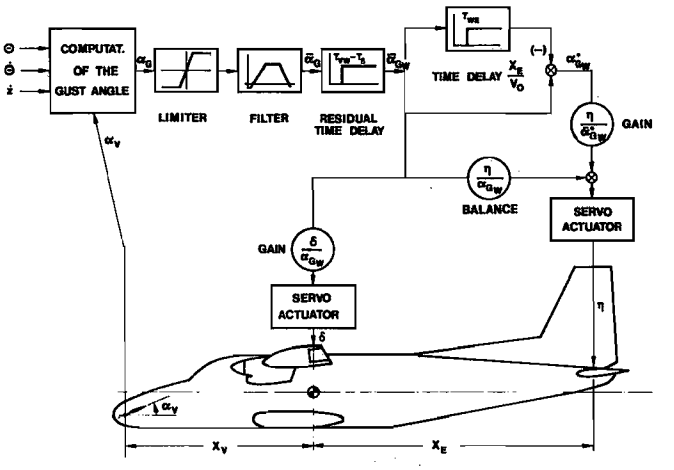

Figure 12. Block diagram of the OLGA gust alleviation system.

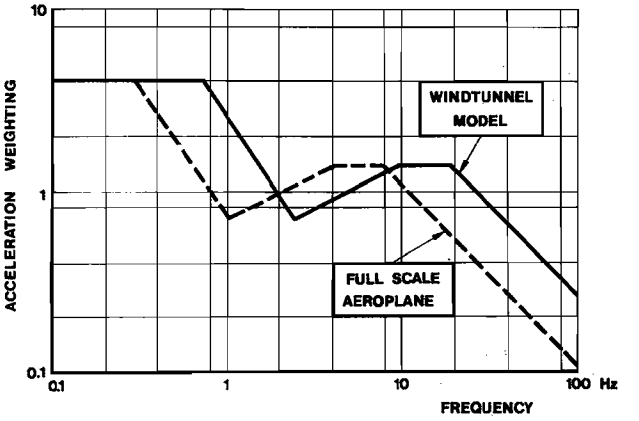

Figure 13. Acceleration weighting function.

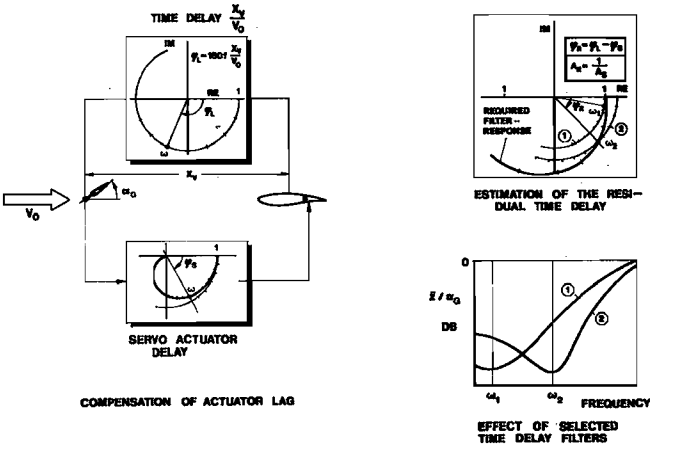

Figure 14. Adjustment of the gust alleviation system (GAS).

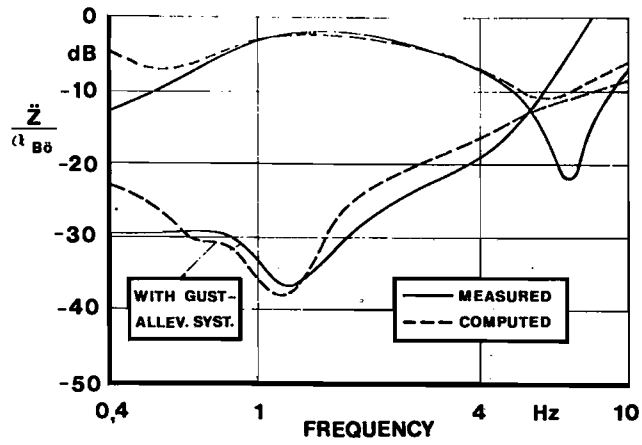

Figure 15. Frequency response of the vertical acceleration. Effect of the gust alleviation system.

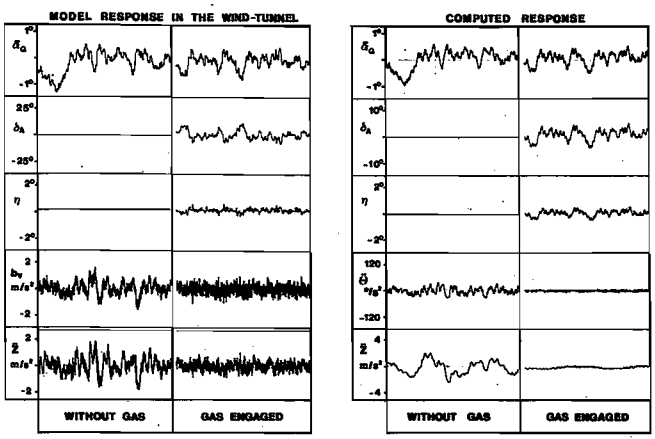

Figure 16. Computed and measured time histories during the flight in a scaled stochastic gust field.

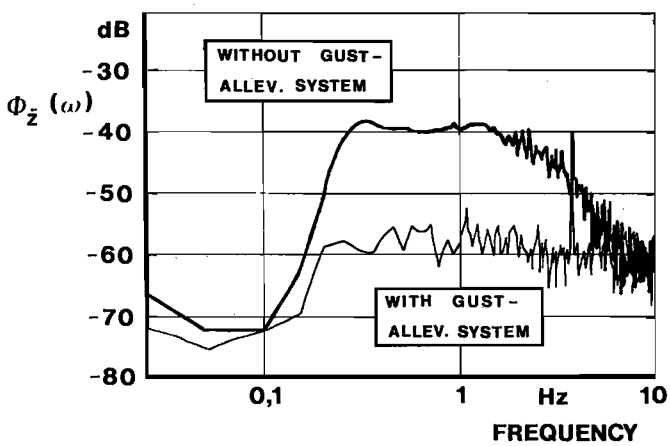

Figure 17. Measured power spectra of the vertical acceleration.

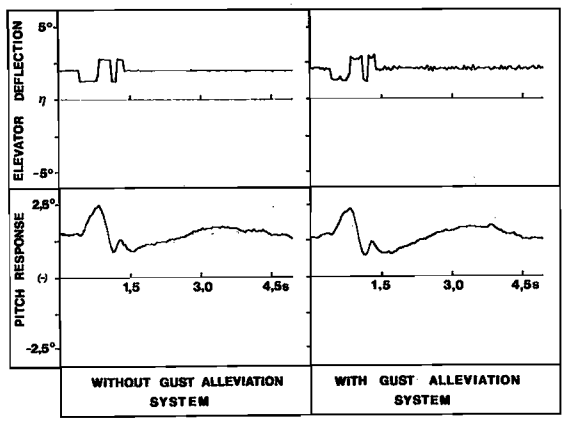

Figure 18. Influence of the gust alleviation system on the handling qualities of the model.

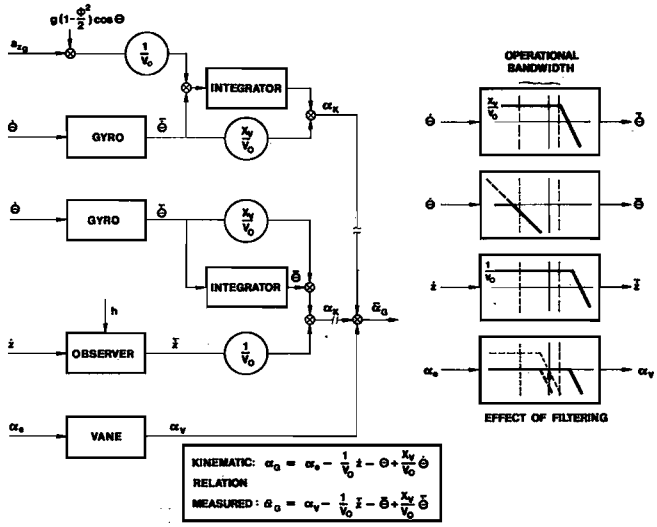

Figure 19. Estimation of the disturbance input signal α_G.

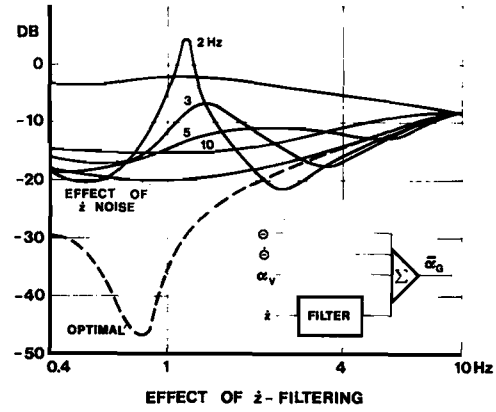

EFFECT OF ż - FILTERING

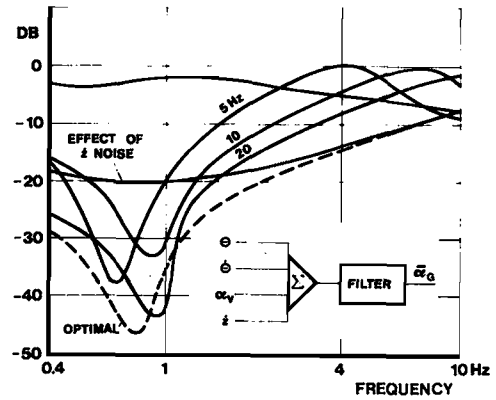

EFFECT OF $\bar{\alpha}_G$ FILTERING

Figure 20. Frequency response of the vertical acceleration. Effect of ż-noise filtering on the gust alleviation system.

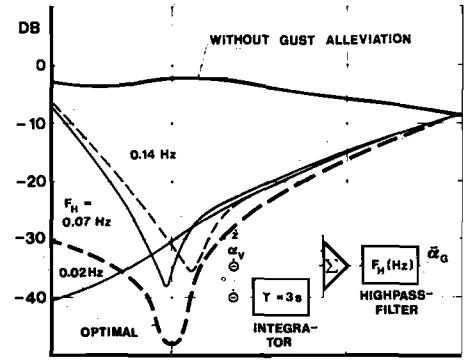

EFFECT OF INTEGRATION TIME CONSTANT AND HIGHPASSFILTER – FREQUENCY

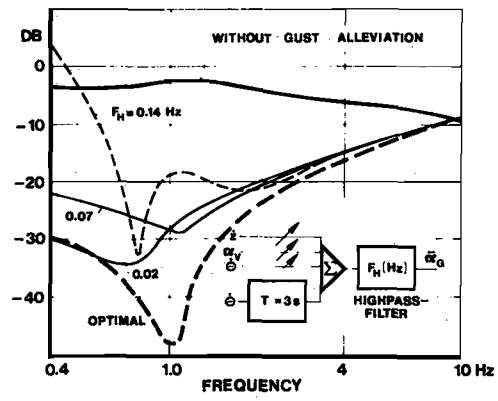

EFFECT OF GUST-SIGNAL $\bar{\alpha}_G$ ADJUSTMENT

Figure 22. Frequency response of the vertical acceleration. Performance of the gust alleviation system with $\dot{\vartheta}$-integration and $\bar{\alpha}_G$-high-pass filtering.

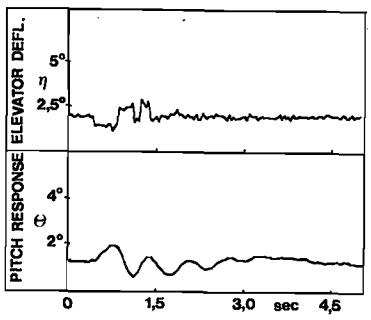

EFFECT OF THE 2Hz ż - FILTER ON HANDLING QUALITIES

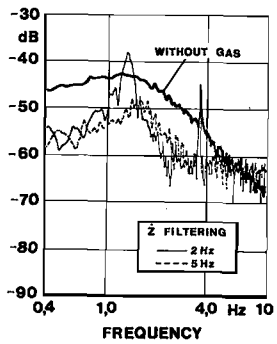

POWER SPECTRUM OF THE VERTICAL ACCELERATION

Figure 21. Effect of ż-filtering on the model response.

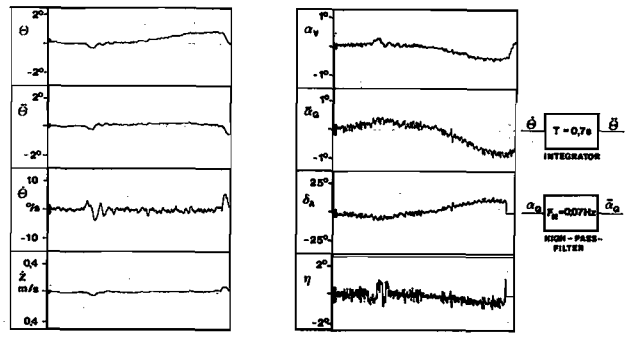

Figure 23. Effect of gust alleviation on handling qualities. Response to elevator impulse during flight in a scaled gust field.

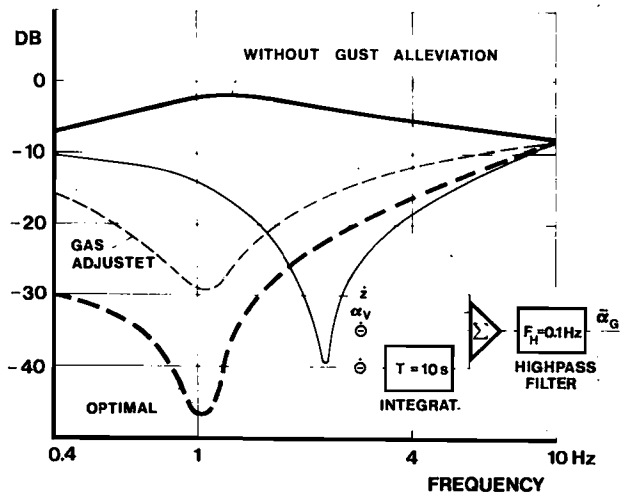

Figure 24. Frequency response of the vertical acceleration. Shifting of the minimum to the desired frequency by adjustment of the GAS-gains and residual time delay.

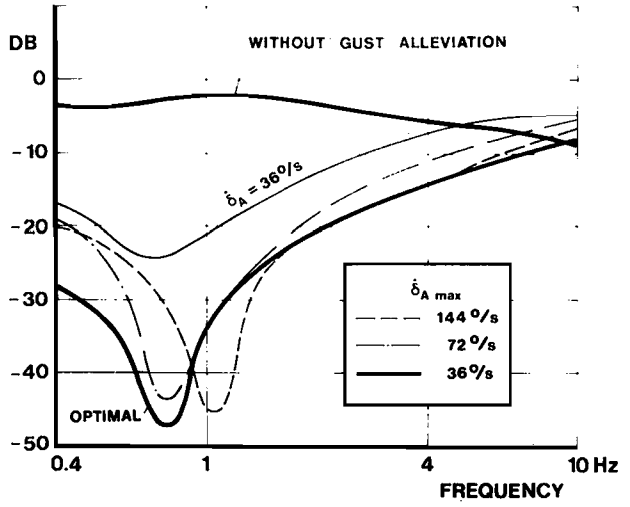

Figure 25. Effect of aileron rate limitation on the performance of the gust alleviation.

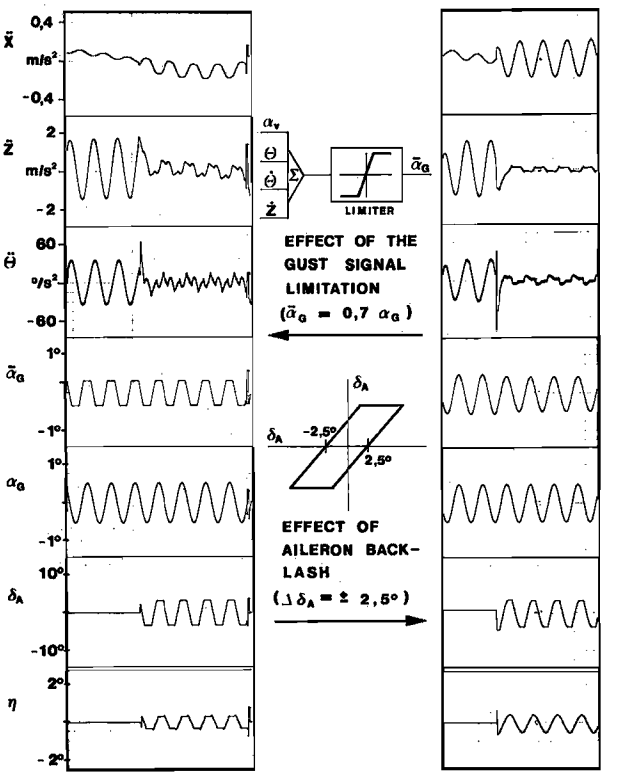

Figure 26. Effect of nonlinearities on the performance of the gust alleviation system.